Calculation of the electron Hall mobility and Hall scattering factor in 6*H*-SiC

G. Ng,[a] D. Vasileska, and D. K. Schroder
Department of Electrical Engineering, Arizona State University, Tempe, Arizona 85287-5706, USA

(Received 4 May 2009; accepted 21 July 2009; published online 15 September 2009)

The calculated electron Hall Mobility and Hall scattering factor in *n*-type 6*H*-SiC based on numerical solutions to the Boltzmann transport equation are presented. These results were obtained by solving the Boltzmann equation exactly for the electron Hall mobility using the contraction mapping principle and the electron drift mobility with Rode's iterative method. The relative importance of the various scattering mechanisms for these calculations is discussed, and a new set of values for the acoustic deformation potential, intervalley deformation potential, and intervalley phonon energy is found, which simultaneously fit experimental Hall mobility and Hall scattering factor data. The calculated Hall mobility and Hall scattering factor are in good agreement with experimental results. In addition, predicted values of the Hall scattering factor for various temperatures and doping concentrations are given. © *2009 American Institute of Physics*.
[doi:10.1063/1.3212532]

I. INTRODUCTION

During the past few decades, the various polytypes of silicon carbide (SiC) have been intensively studied in the hope that it will become a suitable material for high power and high temperature electronic applications. The more developed 6*H* polytype of SiC is already an important substrate material for optoelectronic applications, and, like all SiC polytypes, has garnered attention because its large band gap energy and breakdown voltage make it attractive for high temperature[1] and high power electronics.[2–4] However, for any practical realization of electronic devices on 6*H*-SiC to occur, certain transport properties need to be known. One such quantity is the electron mobility, and, to this end, experimental studies have been carried out to determine its value.[5,6] Along with these experimental results are theoretical calculations that attempt to model them and to explain the mechanisms that determine the mobility.[7–10] Although these computational studies had adequate success in explaining the experimental results, all of these calculations have either (i) focused on calculating the electron drift mobility, while the experimental work has usually measured the electron Hall mobility; or (ii) been inexact solutions based on the relaxation time approximation. Comparisons between the Hall mobility and drift mobility have been justified by either assuming a Hall scattering factor of unity, or through a calculation of the Hall scattering factor, which also relied on the relaxation time approximation. Experiments have shown that the former assumption can be off by as much as 19% depending on temperature and doping concentration.[11] Meanwhile, Hall scattering factors calculated with the relaxation time approximation differ significantly from experimental data.[10]

In this paper a more accurate calculation of the electron Hall mobility and Hall scattering factor for 6*H*-SiC is presented by calculating the electron Hall mobility exactly using the contraction mapping principle.[12] At the same time, the low-field electron drift mobility is solved exactly using the iterative method of Rode,[13–15] and the Hall scattering factor is then arrived at by taking the ratio of the two values multiplied by a mass factor. The various scattering mechanisms are discussed, and a single set of values for the acoustic deformation potential, the intervalley deformation potential, and the intervalley phonon energy, which are adjusted to simultaneously match the experimental Hall scattering factor and Hall mobility data, are given. The calculated electron Hall mobilities and Hall scattering factors are compared with the experimental data of Karmann *et al.*[5] and Rutsch *et al.*,[11] respectively. First, however, a concise overview of the techniques used to solve the Boltzmann transport equation is given.

II. TECHNIQUES FOR SOLVING THE BOLTZMANN TRANSPORT EQUATION

Under steady-state, spatially homogeneous conditions with Fermi–Dirac statistics, the Boltzmann transport equation is given by[13–15]

$$-q\mathbf{F}\cdot\nabla_{\mathbf{k}}f_{\mathbf{k}}=\int[S_{\mathbf{k}',\mathbf{k}}f_{\mathbf{k}'}(1-f_{\mathbf{k}})-S_{\mathbf{k},\mathbf{k}'}f_{\mathbf{k}}(1-f_{\mathbf{k}'})]d\mathbf{k}', \quad (1)$$

where q is the electron charge, $\mathbf{F}$ is the electric field, $f_{\mathbf{k}}$ is the distribution function as a function of wave vector $\mathbf{k}$, and $S_{\mathbf{k},\mathbf{k}'}$ and $S_{\mathbf{k}',\mathbf{k}}$ are the transition rates between states $\mathbf{k}$ and $\mathbf{k}'$. By writing the distribution function as[13–15]

$$f_{\mathbf{k}}=f_0+xg_{\mathbf{k}}, \quad (2)$$

where f_0 is the Fermi–Dirac distribution, $g_{\mathbf{k}}$ is the perturbed distribution function, and x is the direction cosine between $\mathbf{F}$ and $\mathbf{k}$, and inserting into Eq. (1), an iterative form for $g_{\mathbf{k}}$ can be found. This is given by[13–15]

[a]Electronic mail: garrickkng@yahoo.com.

 © 2009 American Institute of Physics

Downloaded 28 Sep 2009 to 129.219.247.33. Redistribution subject to AIP license or copyright; see http://jap.aip.org/jap/copyright.jsp

$$g_{\mathbf{k},i+1} = \frac{S_i(g_{\mathbf{k},i}) + qF\dfrac{df_0}{dk}}{S_o}, \quad (3)$$

and can be solved iteratively for the unknown distribution function by using an initial guess for $g_{\mathbf{k}}$. The operators S_o and $S_i(g_{\mathbf{k},i})$ are the out-scattering and in-scattering rates, respectively. The out-scattering rate is[13–15]

$$S_o = \upsilon_{\text{el}} + 1/\tau_{\text{in}}, \quad (4)$$

where υ_{el} is the sum of the momentum relaxation rates of elastic processes, and $1/\tau_{\text{in}}$ is the sum of the relaxation rates of inelastic processes. The in-scattering rate is[13–15]

$$S_i(g_{\mathbf{k},i}) = \int X g_{\mathbf{k}'}[S^{\text{inel}}_{\mathbf{k}',\mathbf{k}}(1-f_0) + S^{\text{inel}}_{\mathbf{k},\mathbf{k}'}f_0]d\mathbf{k}', \quad (5)$$

where X is the angle between the initial and final wave vectors, and $S^{\text{inel}}_{\mathbf{k}',\mathbf{k}}$ and $S^{\text{inel}}_{\mathbf{k}',\mathbf{k}}$ are the transition rates of the inelastic processes. With the perturbation distribution function $g_{\mathbf{k}}$ solved to arbitrary accuracy, the drift mobility is[13–15]

$$\mu = -\frac{\hbar}{3m^*}\frac{\int \mathbf{k}^3(g_{\mathbf{k}}/F)d\mathbf{k}}{\int \mathbf{k}^2 f_0 d\mathbf{k}}, \quad (6)$$

where μ is the electron drift mobility, $\hbar$ is the reduced Planck constant, and m^* is the effective mass of the electron. This iterative technique to solve for the mobility in the presence of a low electric field was first discussed by Rode in 1973.[13]

A similar technique, also introduced by Rode,[12] solves the Boltzmann transport equation in the presence of an arbitrary magnetic field. In this case, the distribution function is given by[12]

$$f_{\mathbf{k}} = f_0 + xg_{\mathbf{k}} + yh_{\mathbf{k}}, \quad (7)$$

where $h_{\mathbf{k}}$ is the perturbation distribution function due to the magnetic field, and y is the direction cosine from $\mathbf{B}\times\mathbf{F}$ to $\mathbf{k}$. Insertion of Eq. (7) into Eq. (1) yields a coupled pair of equations that can be solved iteratively as[12]

$$g_{\mathbf{k},i+1} = \frac{S_i(g_{\mathbf{k},i}) + qF\dfrac{df_0}{dk} + \beta S_i(h_{\mathbf{k}})}{S_o(1+\beta^2)}, \quad (8)$$

$$h_{\mathbf{k},i+1} = \frac{S_i(h_{\mathbf{k},i}) - \beta qF\dfrac{df_0}{dk} + \beta S_i(g_{\mathbf{k}})}{S_o(1+\beta^2)}, \quad (9)$$

where $\beta = qvB/\hbar kS_o$, v is the electron group velocity, and B is the magnetic field. Using these two perturbed distribution functions, the electron Hall mobility μ_H is[12]

$$\mu_H = \frac{\int \mathbf{k}^3(h_{\mathbf{k}}/B)d\mathbf{k}}{\int \mathbf{k}^3 g_{\mathbf{k}} d\mathbf{k}}. \quad (10)$$

The iterative sequences of Eqs. (8) and (9), as well as Eq. (3), have been shown to be contraction mappings, which guarantee converging solutions.[12]

With the drift mobility and Hall mobility determined, the Hall scattering factor r_H is

$$r_H = \frac{\mu_H}{\mu}. \quad (11)$$

This solution is a more accurate calculation of the Hall scattering factor compared to the more commonly used expression

$$r_H = \frac{\langle\langle \tau^2\rangle\rangle}{\langle\langle \tau\rangle\rangle^2}, \quad (12)$$

where $\langle\langle \tau^2\rangle\rangle$ and $\langle\langle \tau\rangle\rangle$ are the specially averaged scattering times. The latter expression for the Hall scattering factor is derived from the relaxation time approximation, which assumes that scattering times are independent of the distribution function. More importantly, the relaxation time approximation is only valid when the scattering processes are either elastic or isotropic, which is not true for 6*H*-SiC where polar optical phonon scattering dominates the low-field mobility (this scattering mechanism is neither elastic nor isotropic).

III. SCATTERING MECHANISMS IN 6*H*-SIC

In order to calculate S_i and S_o and properly determine the Hall and drift mobilities, the relevant scattering mechanisms must be taken into account. For this study, six scattering mechanisms are considered: (i) acoustic deformation potential scattering, (ii) ionized impurity scattering, (iii) neutral impurity scattering, (iv) piezoelectric scattering, (v) intervalley phonon deformation potential scattering, and (vi) polar optical phonon scattering. The values of the acoustic deformation potential, intervalley phonon deformation potential, and intervalley phonon energy were taken as adjustable parameters to simultaneously fit the Hall scattering factor and Hall mobility data. In addition, parabolic conduction bands are assumed, with the values of the effective masses being $m^*_{M\Gamma}(m^*_1) = 0.75m_0$, $m^*_{MK}(m^*_2) = 0.24m_0$, and $m^*_{ML}(m^*_3) = 1.83m_0$, and the density of states effective mass is $m^* = (m^*_1 m^*_2 m^*_3)^{1/3}$.[16]

Interaction of electrons with nonpolar acoustic phonons results in the acoustic deformation potential scattering. The momentum relaxation rate is given by[13–15,17]

$$\frac{1}{\tau_{\text{ac}}} = \frac{D^2_{\text{ac}} m^* \sqrt{2m^* E_k}}{\pi\hbar \upsilon_S^2 \rho}, \quad (13)$$

where D_{ac} is the acoustic deformation potential, E_k is the carrier energy, υ_S is the longitudinal acoustic velocity, and ρ is the mass density. For 6*H*-SiC, $\upsilon_S = 13\,730\ \text{m/s}^2$ and $\rho = 3211\ \text{kg/m}^3$.[18] As previously stated, D_{ac} is treated as an adjustable parameter to fit experimental data (discussed later) and found to be 5.5 eV.

Coulomb scattering by ionized impurities, important at low temperatures and high doping concentrations, is handled through the Brooks and Herring approach. The momentum relaxation rate is given by[13–15,17]

$$\frac{1}{\tau_{ii}} = \frac{N_I q^4}{16\sqrt{2m^*}\pi\kappa_0^2\varepsilon_0^2 E_k^{3/2}}\left[\ln(1+\gamma^2) - \frac{\gamma^2}{1+\gamma^2}\right], \quad (14)$$

where N_I is the ionized impurity concentration, κ_0 is the low frequency dielectric constant, ε_0 is the permittivity of free space, and $\gamma^2 = 8m^* E_k L_D^2/\hbar^2$. The Debye length L_D is

Downloaded 28 Sep 2009 to 129.219.247.33. Redistribution subject to AIP license or copyright; see http://jap.aip.org/jap/copyright.jsp

$$L_D = \sqrt{\frac{\kappa_0 \varepsilon_0 k_B T}{q^2 N_I}}, \tag{15}$$

where k_B is the Boltzmann constant and T is the temperature. For 6*H*-SiC, the value of the relative dielectric constant is $\kappa_0=9.7$.[18]

Because of the large ionization energies of nitrogen donors in 6*H*-SiC, neutral impurity scattering makes a considerable contribution to the total scattering rate, especially at low temperatures and high doping concentrations. For neutral impurity scattering, the form proposed by Sclar was used, with the momentum relaxation rate given by[17]

$$\frac{1}{\tau_{ni}} = \frac{2^{3/2}\pi\hbar^2 N_I}{m^{*3/2}}\left(\frac{E_k^{1/2}}{E_k+E_T}\right), \tag{16}$$

where the binding energy is $E_T=0.75(m^*/m)(1/\kappa_0)^2$ eV.

Silicon carbide crystals lack inversion symmetry, and are therefore piezoelectric.[19,20] Thus polar acoustic interactions play a role, especially at lower temperatures. The momentum relaxation rate for this process is given by[13,15,17]

$$\frac{1}{\tau_{pz}} = \frac{K^2 q^2 m^{*1/2} k_B T}{2^{3/2}\pi\hbar^2 \kappa_0 \varepsilon_0 E_k^{1/2}}\left[1+\frac{1}{1+\gamma^2}-\frac{\hbar^2}{4m^* L_D^2 E_k}\ln(1+\gamma^2)\right]. \tag{17}$$

For the mobility with the electric field perpendicular to the c axis of the crystal, the coupling coefficient K for wurzite structures is[13,15,17]

$$K^2 = \frac{4(21e_{15}^2+6e_{15}e_x+e_x^2)}{105\kappa_0\varepsilon_0 c_t} + \frac{(21e_{33}^2-24e_{33}e_x+5e_x^2)}{105\kappa_0\varepsilon_0 c_l}, \tag{18}$$

where $e_x=e_{33}-e_{31}-2e_{15}$, and e_{15}, e_{31}, and e_{33} are the piezoelectric constants. The averaged transverse and longitudinal elastic constants for wurzite structures, c_t and c_l, are[13,15,17]

$$c_l = \frac{8c_{11}+4c_{13}+3c_{33}+8c_{44}}{15}, \tag{19}$$

$$c_t = \frac{2c_{11}-4c_{13}+2c_{33}+7c_{44}}{15}, \tag{20}$$

where c_{11}, c_{13}, c_{33}, and c_{44} are the elastic constants. In this study, the piezoelectric constants calculated by Mirgorodsky *et al.*[20] are used, while the elastic constants measured by Kamitani *et al.*[21] are used.

The last two scattering mechanisms, intervalley phonon scattering and polar optical phonon scattering, are inelastic processes. Therefore, in addition to the scattering rates, the integral of Eq. (5) must be evaluated for each of the transition rates. The relaxation rate for intervalley phonon scattering is given by[13–15,17]

$$\frac{1}{\tau_{if}} = \frac{ZD_{if}^2 m^{*3/2}}{\sqrt{2}\pi\hbar^3\omega_{if}\rho}\left[N_i\sqrt{E_k+\hbar\omega_{if}-\Delta E_{fi}} + (N_i+1)\sqrt{E_k-\hbar\omega_{if}-\Delta E_{fi}}\right], \tag{21}$$

where Z is the number of final valleys, D_{if} is the intervalley deformation potential, $\hbar\omega_{if}$ is the intervalley phonon energy, N_i is the intervalley phonon occupation number determined by Bose–Einstein statistics, and ΔE_{fi} is the energy separation between the bottom of the conduction bands of the final and initial valleys. Here we only consider equivalent intervalley scattering, so $Z=4$ and $\Delta E_{fi}=0$.[22] As will be discussed later, fits of experimental data yield $D_{if}=1.25\times10^{11}$ eV/m and $\hbar\omega_{if}=65$ meV. For the in-scattering operator, the integral of Eq. (5) vanishes for intervalley phonon scattering.[13]

Finally, for polar optical phonon scattering, the momentum relaxation rate is given by[13–15,17]

$$\frac{1}{\tau_{\text{pop}}} = \frac{q^2\omega_o m^{*1/2}}{2^{5/2}\pi\varepsilon_0\hbar E_k^{1/2}}\left(\frac{1}{\kappa_\infty}-\frac{1}{\kappa_0}\right)\left[N_o \ln\left|\frac{\sqrt{E_k+\hbar\omega_o}+\sqrt{E_k}}{\sqrt{E_k+\hbar\omega_o}-\sqrt{E_k}}\right| + (N_o+1)\ln\left|\frac{\sqrt{E_k-\hbar\omega_o}+\sqrt{E_k}}{\sqrt{E_k-\hbar\omega_o}-\sqrt{E_k}}\right|\right], \tag{22}$$

where κ_∞ is the high frequency dielectric constant, $\hbar\omega_o$ is the polar optical phonon energy, and N_o is the polar optical phonon occupation number. The polar optical phonon energy is taken to be 120 meV. For the in-scattering operator, the result of Eq. (5) for the polar optical phonon transition rate is[13]

$$S_i = \{N_o g(E_k-\hbar\omega_o)\lambda^- + (N_o+1)g(E_k+\hbar\omega_o)\lambda^+\}, \tag{23}$$

$$\lambda^- = \frac{q^2\omega_o m^{*1/2}}{2^{5/2}\pi\varepsilon_0\hbar E_k^{1/2}}\left(\frac{1}{\kappa_\infty}-\frac{1}{\kappa_0}\right) \times\left(\frac{2E_k-\hbar\omega_o}{[E_k(E_k-\hbar\omega_o)]^{1/2}}\ln\left|\frac{\sqrt{E_k-\hbar\omega_o}+\sqrt{E_k}}{\sqrt{E_k-\hbar\omega_o}-\sqrt{E_k}}\right|-1\right), \tag{24}$$

$$\lambda^+ = \frac{q^2\omega_o m^{*1/2}}{2^{5/2}\pi\varepsilon_0\hbar E_k^{1/2}}\left(\frac{1}{\kappa_\infty}-\frac{1}{\kappa_0}\right) \times\left(\frac{2E_k+\hbar\omega_o}{[E_k(E_k+\hbar\omega_o)]^{1/2}}\ln\left|\frac{\sqrt{E_k+\hbar\omega_o}+\sqrt{E_k}}{\sqrt{E_k+\hbar\omega_o}-\sqrt{E_k}}\right|-1\right). \tag{25}$$

To see the relative importance of each of the scattering mechanisms in n-type 6*H*-SiC, the scattering rates for doping concentrations of $N_D=10^{16}$ cm^{-3} and $N_D=10^{19}$ cm^{-3} are shown in Figs. 1 and 2, respectively, as a function of energy for two different temperatures. Previous studies have indicated that the ratio of impurities at cubic sites to impurities at hexagonal sites is about 2:1.[5,6,11] Therefore, for both of these plots, it is assumed that there are twice as many impurities at cubic sites than there are at cubic sites, and that there is no compensation. The free electron concentration is found by solving the charge neutrality equation

$$n+N_A = \frac{N_{DH}}{1+g_H\exp[(E_F-E_C+E_{DH})/(k_BT)]} + \frac{N_{DK}}{1+g_K\exp[(E_F-E_C+E_{DK})/(k_BT)]}, \tag{26}$$

where n is the electron concentration, N_A is the acceptor compensation level, E_C is the conduction band minimum, E_F is the energy of the Fermi level, N_{DH} and N_{DK} are the concentrations of impurities at hexagonal and cubic sites, re-

Downloaded 28 Sep 2009 to 129.219.247.33. Redistribution subject to AIP license or copyright; see http://jap.aip.org/jap/copyright.jsp

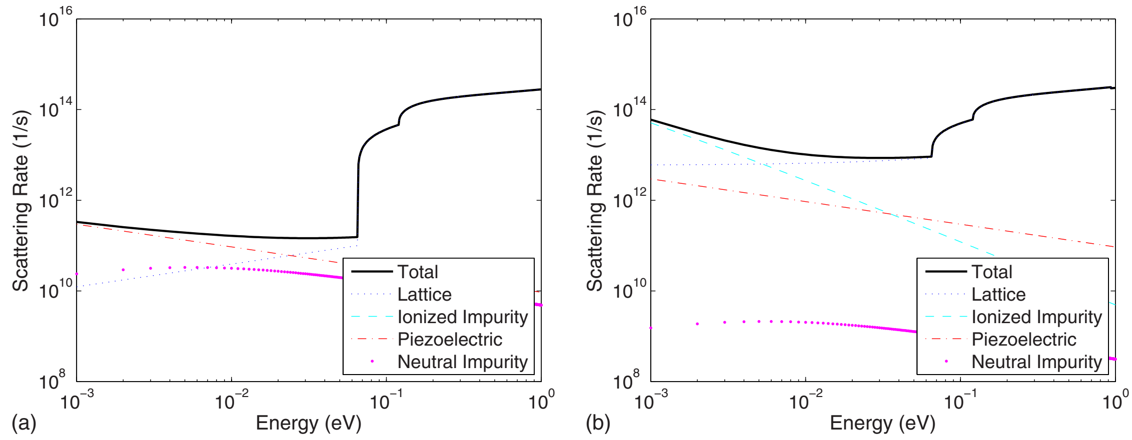

FIG. 1. (Color online) Scattering rates vs energy for $N_D=1\times10^{16}$ cm^{-3} at (a) 30 and (b) 300 K.

spectively, g_H and g_K are the donor degeneracy levels of the hexagonal and cubic levels, respectively, and E_{DH} and E_{DK} are the ionization energies of the impurities at hexagonal and cubic sites, respectively. Both the donor degeneracy levels are assumed to be 2. For this example, the donor ionization energies were set at 94 and 118 meV for the hexagonal and cubic sites, respectively. The lattice scattering in these plots includes acoustic deformation potential, intervalley phonon, and polar optical phonon scattering. At lower temperatures for both doping concentrations, neutral impurity scattering is significant for lower energy carriers, necessitating its inclusion as a scattering mechanism. In addition, at lower temperatures, piezoelectric scattering is the strongest scattering mechanism at lower doping concentrations while still being significant at higher doping concentrations for low energy carriers. All previous mobility and Hall scattering factor calculations have left this mechanism out, even while making calculations at lower temperatures.[7–10] At higher temperatures, ionized impurity scattering generally dominates. For lower doping concentrations, lattice scattering makes a significant contribution, while at higher doping concentrations, neutral impurity scattering is again important.

IV. ELECTRON HALL MOBILITY AND HALL SCATTERING FACTOR

Using Eq. (11) and the techniques discussed in Sec. II, and including the scattering mechanisms discussed above, the Hall mobility and the Hall scattering factor were calculated and were fitted to the experimental data measured by Karmann *et al.*[5] and Rutsch *et al.*[11] These were calculated assuming a measurement configuration of $[\mathbf{B}\parallel\mathbf{c},\mathbf{j}\perp\mathbf{c}]$ and with magnetic fields of $B=0.4$ T and $B=0.741$ T, as in the experiments. Because of the measurement configuration, a mass factor is included in the Hall scattering factor.[10]

As previously mentioned, the values of the acoustic deformation potential, intervalley deformation potential, and intervalley phonon energy were adjusted to obtain a best fit for the Hall mobility and Hall scattering factor data simultaneously. In a manner similar to previous studies,[10,23] the parameters were first adjusted to the Hall mobility data, and then subsequently used in the calculation of the Hall scattering factor data. For the most part, adjustment of the acoustic deformation potential had the effect of shifting the Hall mobility curve higher or lower. Meanwhile, adjustment of the intervalley deformation potential and the intervalley phonon energy primarily affected the slope of the data at temperatures above 100 K. Figure 3 shows the comparison of the calculated and the experimental Hall mobility for three different samples, while Fig. 4 shows the comparison of the calculated and the experimental Hall scattering factor. The calculated results fit the experimental data very well. This is particularly true for the calculated Hall scattering factor, which matches experimental data more so than calculations with a relaxation time approximation by Iwata and Itoh.[10]

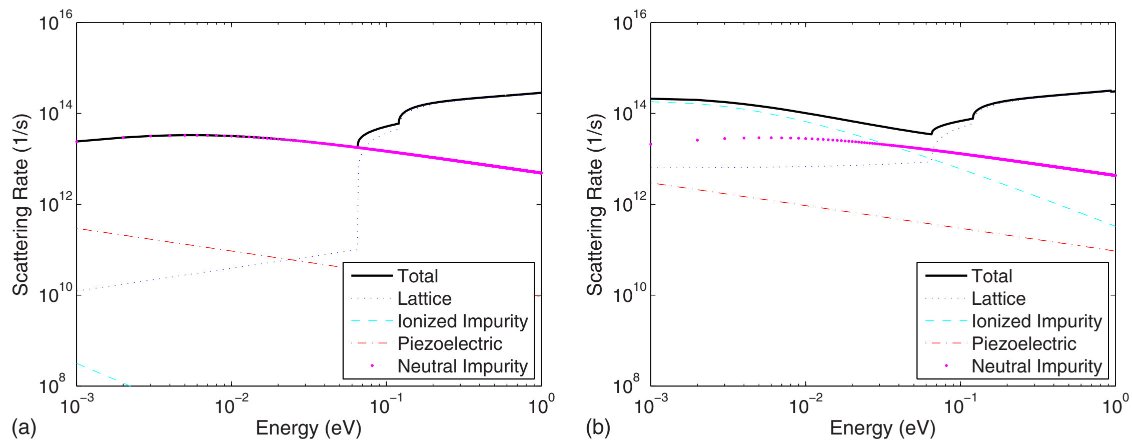

FIG. 2. (Color online) Scattering rates vs energy for $N_D=1\times10^{19}$ cm^{-3} at (a) 30 and (b) 300 K.

Downloaded 28 Sep 2009 to 129.219.247.33. Redistribution subject to AIP license or copyright; see http://jap.aip.org/jap/copyright.jsp

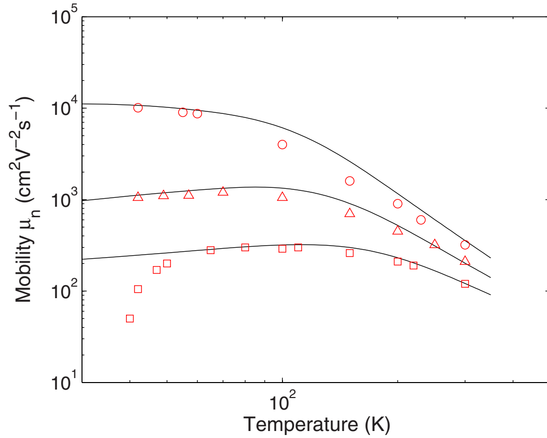

FIG. 3. (Color online) Electron Hall mobility vs temperature at $B=0.4$ T for (a) $N_{DH}=3.5\times10^{15}$ cm^{-3}, $N_{DK}=7\times10^{15}$ cm^{-3}, $N_A=1\times10^{14}$ cm^{-3}, $E_{DH}=94$ meV, and $E_{DK}=118$ meV; (b) $N_{DH}=2\times10^{17}$ cm^{-3}, $N_{DK}=4\times10^{17}$ cm^{-3}, $N_A=1.7\times10^{15}$ cm^{-3}, $E_{DH}=90$ meV, and $E_{DK}=120$ meV; and (c) $N_{DH}=4.4\times10^{16}$ cm^{-3}, $N_{DK}=3.4\times10^{18}$ cm^{-3}, $N_A=5.5\times10^{15}$ cm^{-3}, $E_{DH}=63$ meV, and $E_{DK}=120$ meV n-type 6H-SiC. The solid lines are calculated, while the symbols are experimental data taken from Karmann *et al.* (Ref. 5).

The deviation of the calculated Hall scattering factor in this study from experimental data never exceeds 8.8%.

However, the aforementioned fitting results in values of $D_{ac}=5.5$ eV, $D_{if}=17.5$ eV/m, and $\hbar\omega_{if}=65$ meV, which diverge drastically from previously reported values of $D_{ac}=17.5$ eV, $D_{if}=0.6\times10^{11}$ eV/m, and $\hbar\omega_{if}=85.4$ meV.[7,9] This warrants some discussion. The first study to attempt to extract the deformation potentials and intervalley phonon energy (from which the latter set of parameters originated) by Mickevicius and Zhao[7] used a Monte Carlo method to calculate the electron drift mobility. This calculated mobility was then fitted to experimental Hall data without accounting for the Hall scattering factor. A subsequent study by Dhar and Ghosh[9] used the same set of parameters in a calculation of the drift mobility using Rode's iterative method. The Hall scattering factor in this case was calculated using Eq. (12), which is an inexact solution, and without using a mass factor

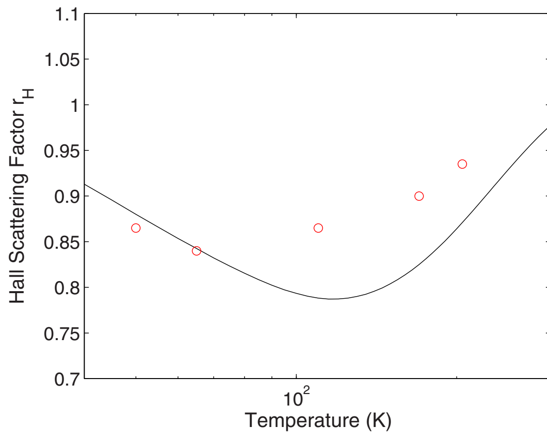

FIG. 4. (Color online) Hall scattering factor vs temperature at $B=0.741$ T for $N_{DH}=3.3\times10^{15}$ cm^{-3}, $N_{DK}=5.7\times10^{15}$ cm^{-3}, $N_A=5.6\times10^{14}$ cm^{-3}, $E_{DH}=112$ meV, and $E_{DK}=157$ meV for n-type 6H-SiC. The solid lines are calculated, while the symbols are experimental data taken from Rutsch *et al.* (Ref. 11).

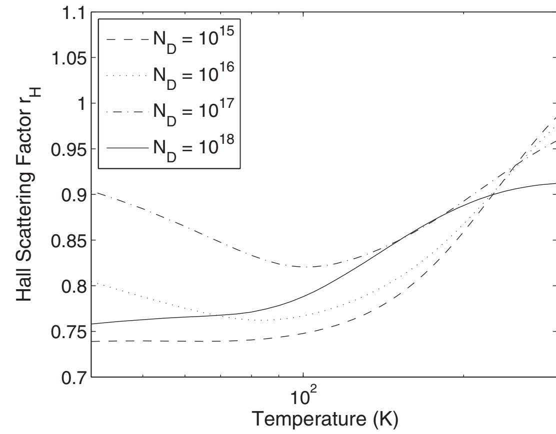

FIG. 5. Predicted values of the Hall scattering factor plotted against temperature with doping concentration as a parameter for n-type 6H-SiC.

to account for the anisotropy of the Hall measurement configuration. It is no surprise that the same set of parameters yields similar results for both the Monte Carlo and Rode's iterative method, as both are recognized as exact methods of obtaining the electron drift mobility. Neither method, however, solves for the Hall mobility. It can therefore be argued that the more accurate parameters are the ones obtained in this study.

Because of the large deviations of the Hall scattering factor from unity and its importance, it is clear that in order to deduce the electron drift mobility from experimental Hall mobility data the Hall scattering factor must be accurately known. Figure 5 shows predicted values of the Hall scattering factor against temperature at four different doping concentrations for $B=0.5$ T. These calculated values assume a 2:1 ratio of impurities at cubic sites to impurities at hexagonal sites, and a compensation ratio of $N_A/N_D=0.01$. These curves show that the doping concentration and the temperature both greatly impact the Hall scattering factor for the $[\mathbf{B}\parallel\mathbf{c},\mathbf{j}\perp\mathbf{c}]$ Hall measurement configuration, so that extreme care must be taken when trying to extract the electron drift mobility from Hall measurements in 6H-SiC.

V. SUMMARY

As previous experimental works have shown, the differences between the Hall mobility and drift mobility in 6H-SiC are not trivial. Nevertheless, the computational studies in this area have usually not completely addressed all the factors pertaining to these differences. This paper studied the Hall mobility and Hall scattering factor of 6H-SiC in detail and to a greater degree of accuracy than previous works. To this end, an examination of the importance of the various scattering mechanisms in 6H-SiC was carried out. Using the contraction mapping principle, the Hall mobility and Hall scattering factor were solved for exactly, and calculated to fit experimental data. From this fitting, a new set of values for the acoustic deformation potential, intervalley deformation potential, and intervalley phonon energy was determined. These values differed significantly from those of previous works, and this is attributed to the more accurate method of calculating the Hall mobility. Finally, the Hall scattering

Downloaded 28 Sep 2009 to 129.219.247.33. Redistribution subject to AIP license or copyright; see http://jap.aip.org/jap/copyright.jsp

factor at different temperatures for various impurity concentrations was calculated in order to aid the extraction of the electron drift mobility from experimental Hall measurements.

[1]D. Chalabi, A. Saidane, M. Idrissi-Benzohra, and M. Benzohra, Microelectron. J. **40**, 891 (2009).
[2]G. Brezeanu, M. Badila, B. Tudor, J. Millan, P. Godignon, F. Udrea, G. A. J. Amaratunga, and A. Mihaila, IEEE Trans. Electron Devices **48**, 2148 (2001).
[3]S. R. Pattanaik, G. N. Dash, and J. K. Mishra, Semicond. Sci. Technol. **20**, 299 (2005).
[4]K. S. Kelkar, N. E. Islam, C. M. Fessler, and W. C. Nunnally, J. Appl. Phys. **98**, 093102 (2005).
[5]S. Karmann, W. Suttrop, A. Schoner, M. Schadt, C. Haberstroh, F. Engelbrecht, R. Helbig, and G. Pensl, J. Appl. Phys. **72**, 5437 (1992).
[6]M. Schadt, G. Pensl, R. P. Devaty, W. J. Choyke, R. Stein, and D. Stephani, Appl. Phys. Lett. **65**, 3120 (1994).
[7]R. Mickevicius and J. H. Zhao, J. Appl. Phys. **83**, 3161 (1998).
[8]T. Kinoshita, K. M. Itoh, M. Schadt, and G. Pensl, J. Appl. Phys. **85**, 8193 (1999).
[9]S. Dhar and S. Ghosh, J. Appl. Phys. **88**, 6519 (2000).
[10]H. Iwata and K. M. Itoh, J. Appl. Phys. **89**, 6228 (2001).
[11]G. Rutsch, R. P. Devaty, W. J. Choyke, D. W. Langer, and L. B. Rowland, J. Appl. Phys. **84**, 2062 (1998).
[12]D. L. Rode, Phys. Status Solidi B **55**, 687 (1973).
[13]D. L. Rode, Semicond. Semimetals **10**, 1 (1973).
[14]M. Lundstrom, *Fundamentals of Carrier Transport* (Cambridge University Press, Cambridge, 2000).
[15]D. K. Ferry, *Semiconductor Transport* (Taylor & Francis, New York, 2000).
[16]C. Persson and U. Lindefelt, Phys. Rev. B **54**, 10257 (1996).
[17]B. K. Ridley, *Quantum Processes in Semiconductors* (Oxford Science, Oxford, 1999).
[18]Y. Goldberg, M. E. Levinshtein, and S. L. Rumyanstev, *Properties of Advanced Semiconductor Materials: GaN, AlN, InN, BN, SiC, SiGe* (Wiley Interscience, New York, 2001).
[19]S. Karmann, R. Helbig, and R. A. Stein, J. Appl. Phys. **66**, 3922 (1989).
[20]A. P. Mirgorodsky, M. B. Smirnov, E. Abdelmounim, T. Merle, and P. E. Quintard, Phys. Rev. B **52**, 3993 (1995).
[21]K. Kamitani, M. Grimsditch, J. C. Nipko, C. K. Loong, M. Okada, and I. Kimura, J. Appl. Phys. **82**, 3152 (1997).
[22]H. Iwata, K. M. Itoh, and G. Pensl, J. Appl. Phys. **88**, 1956 (2000).
[23]G. Rutsch, R. P. Devaty, W. J. Choyke, D. W. Langer, L. B. Rowland, E. Niemann, and F. Wischmeyer, Mater. Sci. Forum **338**, 733 (2000).

Downloaded 28 Sep 2009 to 129.219.247.33. Redistribution subject to AIP license or copyright; see http://jap.aip.org/jap/copyright.jsp